

FLAPPING MOTION OF A SUPERSONIC RECTANGULAR JET, A REDUCED ORDER MODEL STUDY

Vincent Jaunet
v.jaunet@etu.univ-poitiers.fr

Erwan Collin
erwan.collin@ensma.fr

Joel Delville
PPRIME Institute-UPR 3346
CNRS - University of Poitiers - ENSMA
joel.delville@pprime.fr

ABSTRACT

This article describes an aeroacoustic feedback resonant mechanism observed in a rectangular supersonic jet operating at off design conditions. Strong acoustic waves, that have a narrow band non-linear behavior, are observed in the external flow field and the jet undergoes a strong coherent flapping motion.

A low order model study, based on POD analysis, is performed on dual-time schlieren visualization, allowing to relate the external acoustic waves and the coherent motion of the jet.

The main characteristics of this aero-acoustic feedback loop are investigated and it is shown that the behavior of the jet is not exactly similar to the well known screech phenomenon. Differences between the case studied here and a classical screech phenomenon are then discussed.

Introduction

Choked nozzles as well as convergent-divergent ones operated at off-design conditions are known to produce an intense and narrow band shock noise, referred to as *jet screech* that can induce severe structural loading. Jet screech tone consists in a resonant, aeroacoustic feedback loop first described by Powell (1953*b,a*). This feedback loop can be considered as an external acoustic wave that propagates upstream (the outer loop), and disturbances generated in the jet mixing layer that grow while being convected downstream (the inner loop). As the jet exits at off design conditions, the convected disturbances interact with the shock cells of the flow and generate new acoustic waves that continue the feedback resonant loop. A review of this phenomenon can be found in Raman (1999).

A simple relationship, first derived by Powell (1953*b*) and Tam *et al.* (1986), and later improved to account for flight speed effects by Tam (1991), has been shown to accurately predict screech tone frequency, and is given by:

$$f_s = \frac{U_c}{L_s [1 + U_c / (a_\infty (1 - M_e))]}, \quad (1)$$

where f_s is the screech tone frequency, L_s refers to the shock cell spacing, M_e represents the external Mach number, a_∞

is the external speed of sound and U_c is the convective velocity of the disturbances in the jet mixing layer.

Thus the prediction of the screech tone frequency can be completed by the knowledge of shock cell spacing L_s and the convective velocity U_c . For rectangular jets, Tam (1988) provided an explicit solution for the shock cell spacing which is given by:

$$L_s = \frac{2 (M_{fe}^2 - 1)^{1/2} h_{fe}}{[1 + (h_{fe}^2 / b_{fe}^2)]^2}, \quad (2)$$

with h_{fe} and b_{fe} being the small and long dimensions of the fully expanded nozzle, and M_{fe} is the fully expanded Mach number. Concerning the convective speed of the disturbances U_c , it is usually taken to be between $0.5U_j$ and $0.7U_j$. Alksilar *et al.* (2003) found it to be equal to $0.5U_j$ in over-expanded conditions and equal to $0.63U_j$ in under-expanded cases. Therefore, the use of the former equations allows to evaluate the screech tone frequency for simple rectangular jet.

Recently, Jaunet *et al.* (2010) proposed to use a modified nozzle in order to vectorize a rectangular jet by fluidic actuation. The modifications of the nozzle consisted in the addition of secondary divergents at the vicinity of the exit section of the nozzle, that locally accelerates the flow through centered expansion waves. As a consequence, the jet cannot run in fully adapted regime. Furthermore, it turned out that this jet, even unmanipulated, underwent a strong flapping motion that can be due to a resonance between acoustics in the external flow and the flow itself, such as a screech mechanism. Thus, this article describes this feedback resonant mechanism.

The outer-loop of the screech (the acoustics propagating in the subsonic flow) is investigated by means of pressure sensing. Spectral analysis are performed giving a clue in understanding the main features of the acoustics outer-loop. Then, the inner-loop (within the mixing layer) is investigated with dual-time schlieren visualizations and Proper Orthogonal Decomposition. The first part of this paper describes the experimental set-up. The second one aims at describing the resonant feedback loop observed. Then a discussion is given highlighting the role of three-

dimensionality of the flow on the resonant loop.

Experimental set-up Wind tunnel

Experiments were conducted in the S150 wind tunnel of the PPRIME Institute of Poitiers. They consist of a Mach number $M = 1.45$ supersonic rectangular jet of $h = 30$ mm wide and $b = 150$ mm height. The geometry of the nozzle is lightly modified by the addition of two small divergents, initially designed in order to study possibilities of fluidic thrust vectoring. These divergents are made by 10° slopes of the wall with respect to the main flow direction. They occupy the whole width of the nozzle and are 30 mm long, which length is equal to the width of the nozzle.

As the air flows at supersonic speed, an expansion fan is generated on the corner. Therefore, the pressure of the flow at the exit section of the nozzle is not uniformly distributed and the fully adapted regime cannot be reached. Thus, the stagnation pressure was chosen as the minimum pressure necessary to ensure full flowing conditions. It was checked that the flow do not separate from the wall before the exit section with oil flow visualizations.

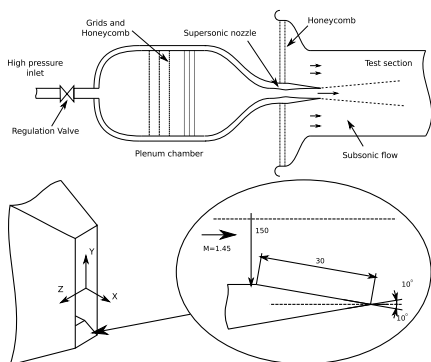


Figure 1. Schematic diagram of the wind tunnel and detail of the supersonic nozzle.

The jet is exiting in a square shaped subsonic wind tunnel of 500mm high, and the subsonic surrounding flow is obtained through suction of ambient air and flows at a Mach number $M_e = 0.2$

The reference coordinates axis is chosen so that x is aligned with the main flow stream and y is aligned with the long sides of the nozzle. A sketch of the wind tunnel together with a detailed view of the nozzle is given in figure 1. The stagnation conditions and main characteristics of the flow are summarized in the table 1.

Measurements and Visualizations

Unsteady pressure measurements

Two walls of the test section are equipped with Kulite sensors, placed on the $z = 0$ and $y = 0$ planes (*i.e.* on opposite sides, parallel to the long side of the nozzle) at a stream-wise distance of $x = 8 \times h$. A sketch of the localization of the sensors with respect to the flow is given in figure 2.

The pressure signals are acquired simultaneously at a sample rate of 80kHz after being low pass filtered

Table 1. Experimental conditions.

	Supersonic jet	Co-flow
Dimensions (mm)	150×30	500×500
M	1.45	0.2
M_{fe}	1.52	-
U (m/s)	380	60
P_0 (10^5 Pa)	3.7	1
T_0 (K)	260	290

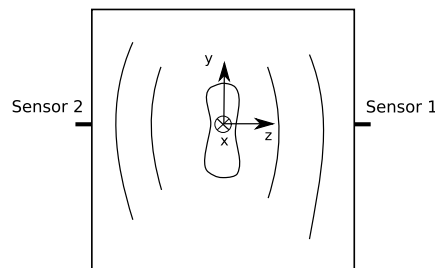


Figure 2. Schematic diagram of the localization of the pressure sensors

with a cut-off frequency of 40kHz to avoid any aliasing phenomena, and consisted of 2×10^6 samples. In the following, when pressure data is invoked the subscript i refers to the signal of sensor number i . Then, S_{ii} refers to the auto-spectrum of signal i , and then the subscript ij is used to mention cross-spectra obtained from sensor i and j (same notation is used for the phase ϕ_{ij} , the coherence γ_{ij}^2).

Dual-time spark schlieren photographs

Pairs of instantaneous schlieren visualizations are acquired using a double spark light source together with a Particle Image Velocimetry (PIV) apparatus. Synchronization between the light source and the PIV camera is controlled by a computer. Thus, the time delay between each image can be adjusted up to a minimum of $\Delta t = 1\mu s$. The 12 bits CCD sensor of the camera is composed of 1200×1600 pixels covering a field of view of about $200mm \times 200mm$, so that the resolution is sufficient to study the coherent features of the flow.

The two successive sparks of the light source are obtained with two different pairs of electrodes. Consequently, the two successive images may not possess the same illumination and contrast. This can cause some problem during the post-processing, therefore the energy of each image is normalized and an histogram specification is applied.

An acoustic feedback loop mechanism

An example of schlieren picture of the jet, taken from a small side point of view, is given in the figure 3. Although it is composed of two uncorrelated images, it is clear that the jet is undergoing a very coherent flapping motion in the (x, z) plane. This motion is induced by structures created in the incipient mixing layer, in the vicinity of the nozzle lips.

Some of these structures are visible on figure 3, they are highlighted by dashed white circles. We then see that they grow as they are convected downstream by the flow.

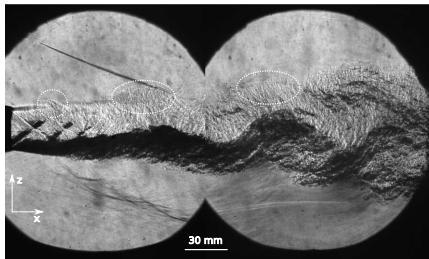


Figure 3. Example of spark schlieren picture composed of two uncorrelated images, taken from the small side point of view of the nozzle.

Furthermore, this figure shows that strong acoustic waves are present in the subsonic part of the flow. These waves are propagating upstream and are responsible of the creation of the structures mentioned above when they reach the nozzle. This behavior is common to all of screeching jets, but one difference that comes here is the direction of propagation of these waves. In a classical screech phenomenon, the acoustic perturbations generally emanate spherically from a downstream location of jet (third or fourth shock cell Raman (1999); Alksilar *et al.* (2003)). But here, the acoustic source location could not be seen and seems to be located far downstream so that the waves first reflect on the wall of the wind tunnel before impinging the nozzle lips.

The wall pressure power spectral density obtained from the sensor number 1, is showed on figure 4. As for a screeching rectangular jet, the energy of the signal is dominated by a fundamental frequency $f_s = 2930\text{Hz}$ and numerous harmonics.

Secondary peaks are visible on both sides of the main peaks. This is a typical behavior of quadratic interactions between two frequency component f_1 and f_2 , leading to the appearance $f_1 - f_2$ and $f_1 + f_2$. Here f_1 is one the screeching tone and f_2 is a very low frequency of about 700 Hz. Actually, Walker & Thomas (1997) explained that this low frequency corresponds to an amplitude modulation of the screech tone, that leads in the Fourier spectrum to the appearance of secondary peaks at $f = f_s \pm 700\text{ Hz}$.

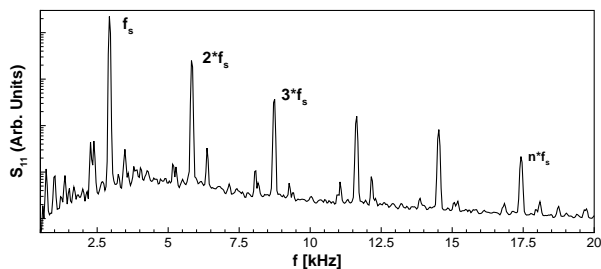


Figure 4. Power spectral density of wall pressure fluctuations inside the wind tunnel. Sensor number 1.

The coherence γ_{12} and phase ϕ_{12} between the signals of sensor 1 and 2 are presented on figure 5. A high level of coherence is visible for the fundamental screech frequency indicating that the phase between the two signals is coherent at this frequency, and is equal to π . This shows that the acoustic excitation of the jet of the present study is organized in an anti-symmetrical mode. This mode has been widely observed in many experiments and numerical simulations Raman & Rice (1993); Gutmark *et al.* (1990); Berland *et al.* (2007), and is the most natural one for rectangular jets flowing at fully expanded Mach number comparable to ours.

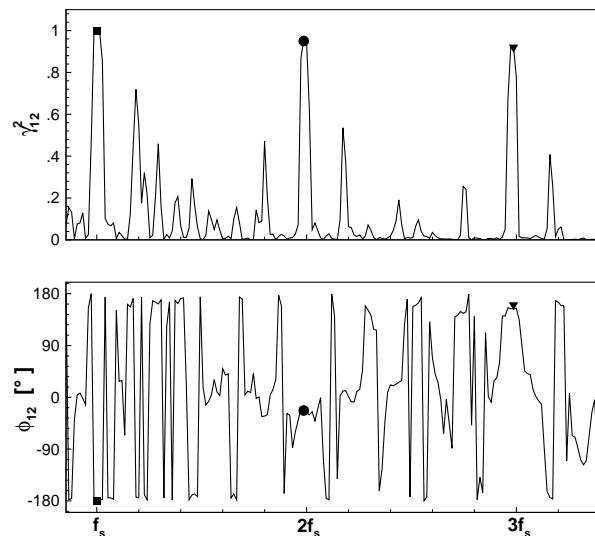


Figure 5. Coherence and phase between sensors 1 and 2.

Thus, the acoustic waves identified in the present study shows a behavior similar to the one in a classical rectangular screeching jet apart from the direction of propagation of the acoustic waves. This may be attributed to the presence of the wind tunnel walls which provides another way to the acoustics to reach the nozzle. In the following, we will provide a study of the aerodynamic behavior of the jet using dual schlieren visualizations, and we will show that the presence of acoustic waves in the subsonic part of the flow is responsible for the flapping motion the jet.

Large scale characteristics of the flow Domain of study and POD analysis

As presented in figure 6, the POD analysis is performed on a subdomain of the original visualizations. This subdomain is chosen in order to take into account that a great part of the photograph do not contain any information about the flow. Moreover, the domain of study is focused on region where the flapping motion of the jet is fully developed. This leads to an analysed domain of size $5 \leq x/h \leq 9.5$ and $-1.6 \leq z/h \leq 1.6$.

The POD decomposition is performed on the fluctuating grayscale level field $g(\mathbf{x}, t)$ and computed using a *Snap*-

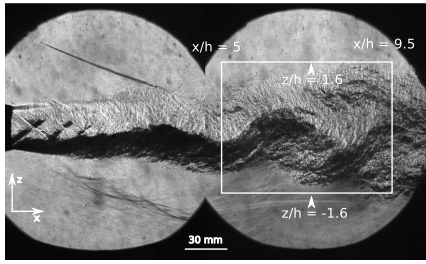


Figure 6. Definition of the domain of interest on which the POD analysis is performed.

shot PODSirovich (1987):

$$g(\mathbf{x}, t) = \sum_{n=1}^{N_s} a^{(n)}(t) \Phi^{(n)}(\mathbf{x}), \quad (3)$$

with N_s representing the total number of POD modes directly given by the number of instantaneous visualizations (200 samples in our case).

As dual-time schlieren photographs were acquired, the time derivative of the temporal modes can be computed through a second-order scheme:

$$a_t^{(n)}(t + \frac{\Delta t}{2}) = \frac{a^{(n)}(t + \Delta t) - a^{(n)}(t)}{\Delta t}, \quad (4)$$

In order to conserve the temporal modes at the same time that their time derivatives, the temporal modes are interpolated. Thus, the temporal modes are calculated with:

$$a^{(n)}(t + \frac{\Delta t}{2}) = \frac{a^{(n)}(t + \Delta t) + a^{(n)}(t)}{2}. \quad (5)$$

Then, the new eigenfunctions are calculated by projecting the velocity field onto the interpolated temporal modes.

The POD eigenspectrum is plotted in figure 7(a). The first 4 POD modes represent 60% of the total energy and are sufficient to produce partial reconstructions of the flow well describing the flapping motion of the flow (see figure 8). As the reader can notice, the energy contents of mode 1 and mode 2 on the one hand, and mode 3 and mode 4 on the other hand, are of the same order of magnitude. That is to say $\lambda^{(1)} \simeq \lambda^{(2)}$ (respectively $\lambda^{(3)} \simeq \lambda^{(4)}$), and this results from the fact that the visualizations well capture the convective motion of the flow.

Actually, the reproduction of a propagating flow pattern from eigenfunctions that are fixed in space needs pairs of eigenfunctions $\Phi^{(n)}(\mathbf{x})$. Therefore, the temporal dynamics of mode 1 and 2 are very similar, the main difference being a simple phase shift of $\pi/2$. This leads to a simple dynamics in the phase space ($a^{(1)} - a^{(2)}$), in which the temporal modes describe a circle (see figure 9(a)). The dynamics of mode 3 and mode 4 is almost the same. In fact, mode 3 and mode 4 described the same dynamics and are simply phase shifted of $\pi/2$. Furthermore, they seem to evolve at twice the pulsation of mode 1 and mode 2 giving the particular path in the phase space shown in figure 9. Therefore, in the following of the paper, we will only consider the 4 first POD modes which well captures the coherent flapping motion of the jet.

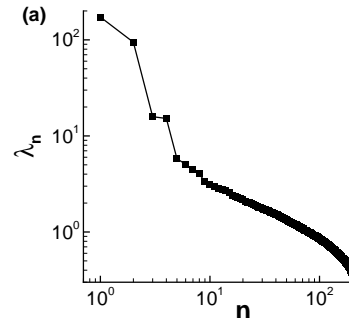


Figure 7. POD eigenspectrum

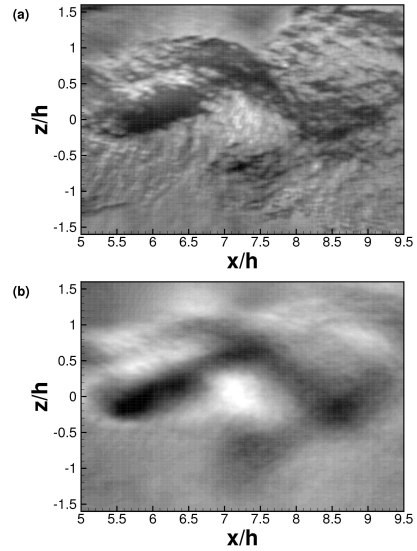


Figure 8. Comparison of original image (a) and its 4 modes partial reconstruction (b).

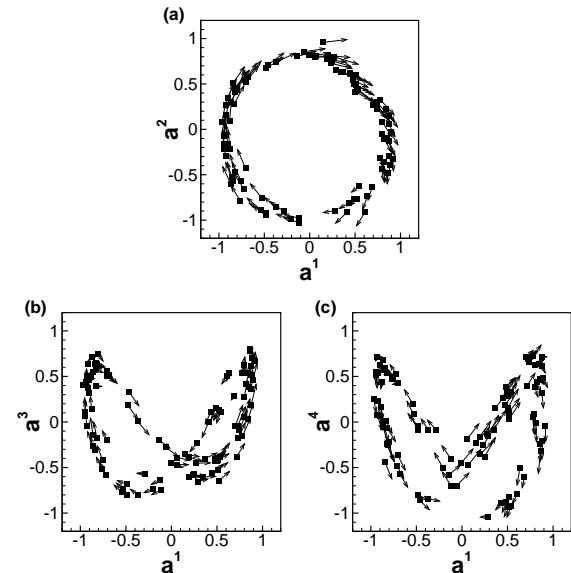


Figure 9. Phase portraits of the first 4 modes. The arrows represent the time derivatives of the modes.

Flapping frequency estimation

Perret *et al.* (2006) succeeded in obtaining the main frequency of the flapping motion of a counterflow jet with the

use of POD analysis. They proposed to consider a linear low order dynamical subsystem only composed of mode 1 and mode 2, which can be written as follows:

$$a_{,t}^{(i)} = L_{ij}a^{(j)} + D_i, \quad (6)$$

where the subscript “,*t*” refers to the time derivative, and with implicit summation over the repeated subscripts. As the temporal modes and their time derivatives are zero-centered, the D_i term can be neglected. Furthermore, in case a strong correlation exists between the time derivative $a_{,t}^{(i)}$ and the mode $a^{(j)}$ (with $i \neq j$), the dynamical system can be reduced to:

$$\begin{cases} a_{,t}^{(1)}(t) = L_{12} a^{(2)} \\ a_{,t}^{(2)}(t) = L_{21} a^{(1)}. \end{cases} \quad (7)$$

This system can easily be integrated thus we find:

$$\begin{cases} a^{(1)}(t) = K_1 \cos(\omega t + \phi_1) \\ a^{(2)}(t) = K_2 \cos(\omega t + \phi_2), \end{cases} \quad (8)$$

with $\omega = \sqrt{-L_{12}L_{21}} = 2\pi f$. Thus, the characteristic frequency of the flow is directly related to L_{12} and L_{21} . These coefficient can be calculated using a linear regression between the temporal modes and their time derivatives as shown in figure 10.

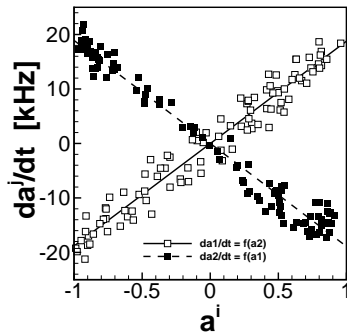


Figure 10. Frequency estimation of the motion of the 2 first modes

We then obtain $L_{12} = 1.88 \times 10^4 s^{-1}$ and $L_{21} = -1.89 \times 10^4 s^{-1}$ giving $f = 3000 Hz$ which is very close to the fundamental frequency of the acoustic waves propagating in the subsonic part of the flow, actually only 2.3% superior. Furthermore, the figure 9 showed that the modes 3 and 4 evolve at a frequency which is twice the frequency of the 2 first modes. It clearly indicates that the modes 3 and 4 captured the first harmonic of the flapping motion of the jet.

Both the external acoustic waves and the flapping motion of the jet are dominated by a common frequency. This can be a sign of a flow dominated by a screech mechanism. However, this *screech tone* seems to be very specific to our flow configuration, due to a particular geometry of the nozzle.

Discussion on the feedback mechanism

In figure 11 is plotted the Strouhal number of the screech $St = f_s U_{fe} / h_{fe}$ against the fully expanded Mach number for Tam's model (Tam, 1988) (equations 1 and 2) and for our experiment. It is obvious that the theory fails in predicting the screeching frequency of the jet of the present study.

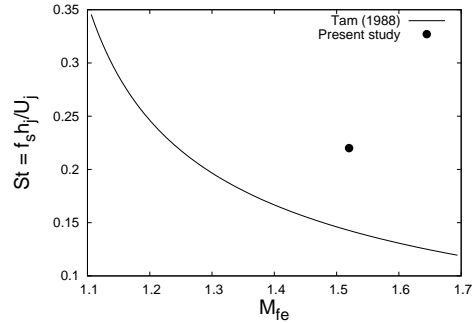


Figure 11. Comparison of theoretical prediction of screech frequency Tam (1988) and our experiment

A reason for this difference can be found in the particular geometry of the shock cell structure of the jet studied here. As mentioned previously, the ending parts of the nozzle have been designed so that they are slightly diverging (see figure 1). Therefore, the jet of this present study is underexpanded in the center of the nozzle and overexpanded at each extremities, leading to a special shock structure.

The figure 12 presents a average schlieren photography taken in plane parallel of the long size of the nozzle superimposed on the centerline mean streamwise velocity of the jet obtained by Particle Image Velocimetry. The schlieren visualization is integrated all along the optical path so that its interpretation has to be done with care. Nevertheless, signs of three-dimensionality are visible on the upper and the lower parts of the first shock wave. This three-dimensionality results from the fact that the exit conditions are not homogeneous in the vertical direction, as it can be seen on the schlieren.

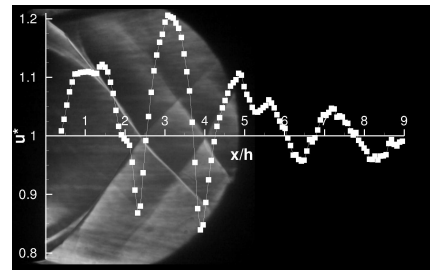


Figure 12. Centerline mean streamwise velocity (PIV) of the jet superposed on a mean schlieren.

The shock cell spacing, taken from the velocity profile presented in figure 12, for the four first cells are summarized in table 2. Thus, only the first and third shock cell have length comparable with the one predicted with the model of

Tam (1988), the second and fourth one are much smaller. Therefore, it seems not possible to reduce the shock cell spacing as a one-dimensional wave of unique length.

Cell	1	2	3	4	Tam (1988)
L_s/h_j	2.2	1.5	2.41	1.83	2.3

Table 2. Measured shock cell spacing of the present jet and predicted one Tam (1988).

Raman (1997) already observed that jet screech fundamental frequency is sensitive to the structure of the shock cell using bevelled nozzle, forcing Tam *et al.* (1997) to perform a bidimensional analysis in order to model the shock cell spacing. Their result showed that, contrary to the conventional rectangular jet where only one wavelength has to be retained, several higher modes are needed in order to reasonably predict the screeching main frequency of jets exiting from beveled nozzles.

Therefore, we may expect that the three-dimensional shock cell structure of the jet of the present study makes the prediction of the screech tone impossible with the usual models.

Conclusion

A study of an aeroacoustic feedback mechanism has been carried out using pressure sensing and schlieren visualizations. It has been shown that slight modifications on the nozzle geometry can induce strong changes in the shock cell pattern of the jet and thus on the screeching frequency of the jet.

It is clear that the test section walls have an influence on the acoustic waves propagation path. Although it has not been possible to precisely locate the emanation point of these waves, a simple study of the acoustic of the test section showed that the frequency involved in feedback loop is not due to the resonance of test section. Thus, the described feedback mechanism is clearly due to the jet, and further study have to be made in order to find out the origin of the acoustic waves.

Dual-time schlieren visualizations combined with POD analysis have been shown to be a simple and precise tool in order to study the main flow scales. Thus, it has been able to prove that the observed flapping motion of the jet occurs at the same frequency as the external acoustic fundamental frequency.

However lots of similarities have been highlighted between the screeching mechanism studied here and the one of a classical rectangular jet, the fundamental frequency of the screeching mechanism could not be predicted using standard prediction models. This has been explained by the fact that the exit section of the jet was not conventional leading to a highly three dimensional flow and shock structure. Many research efforts have been made in the past in order to build models that can predict the fundamental frequency

of such mechanisms. Nevertheless, the presented results showed that if more complex and realistic geometries are involved, these models don't seem to provide a confident prognostic.

acknowledgements

The authors wish to thank the Region Poitou-Charentes and DGA-Spae for supporting part of this study.

REFERENCES

- Alksilar, M. B., Krothapalli, A. & Lourenco, L. M. 2003 Structure of a screeching rectangular jet : a stereoscopic particle image velocimetry study. *Journal of Fluid Mechanics* **489**, 121–154.
- Berland, J., Bogey, C. & Baily, C. 2007 Numerical study of screech generation in a planar supersonic jet. *Physics of fluids* **19**.
- Gutmark, E., Schadow, K. C. & Bicker, C. J. 1990 Near acoustic field and shock structure of rectangular supersonic jets. *AIAA Journal* **28** (7), 1163–1170.
- Jaunet, V., Aymer, D., Collin, E., Bonnet, J.-P., Lebedev, A. & Fourment, C. 2010 3D effects in a supersonic rectangular jet vectored by flow separation control, a numerical and experimental study. *AIAA paper* **2010-4976**.
- Perret, L., Collin, E. & Delville, J. 2006 Polynomial identification of POD based low-order dynamical system. *Journal of turbulence* **7**.
- Powell, A. 1953a On the mechanism of choked jet noise. *Proceedings of the Physical Society of London* **B66**, 1039–1056.
- Powell, A. 1953b On the noise emanating from a two dimensional jet above the critical pressure. *Aeronautical quarterly* **4**, 103–122.
- Raman, G. 1997 Screech tones from rectangular jets with spanwise oblique shock-cell structure. *Journal of Fluid Mechanics* **330**, 141–168.
- Raman, G. 1999 Supersonic jet screech : half-century from powell to the present. *J. of Sound and Vib.* **225**, 543–571.
- Raman, G. & Rice, E. J. 1993 Intability modes excited by natural screech tones in a supersonic rectangular jet. *AIAA Paper AIAA-83-4021*.
- Sirovich, L. 1987 Turbulence and the dynamics of coherent structures. part 1 : coherent structures. *Quarterly of applied mathematics* **XLV**.
- Tam, C. K. W. 1988 The shock-cell structures and screech tone frequencies of rectangular and non-axisymmetric jets. *Journal of Sound and Vibration* **121**, 135–147.
- Tam, C. K. W. 1991 Aeroacoustics of flight vehicles: theory and practice. *Nasa Technical Report 90-3052 1: Noise sources*.
- Tam, C. K. W., Seiner, J. M. & Yu, J. C. 1986 Proposed relationship between broadband shock associated noise and screech tones. *Journal of sound and vibration* **110**, 309–321.
- Tam, C. K. W., Shen, H. & Raman, G. 1997 Screech tones of supersonic jets from bevelled rectangular nozzles. *AIAA Journal* **35** N7, 1119–1125.
- Walker, H.W. & Thomas, F.O. 1997 Experiments characterizing nonlinear shear layer dynamics in a supersonic rectangular jet undergoing screech. *Physics of Fluids* **9**, 2562–2579.